



Direct Writing of a 90 wt% Particle Loading Nanothermite

Haiyang Wang, Jinpeng Shen, Dylan J. Kline, Noah Eckman, Niti R. Agrawal, Tao Wu, Peng Wang, and Michael R. Zachariah*

The additive manufacturing of energetic materials has received worldwide attention. Here, an ink formulation is developed with only 10 wt% of polymers, which can bind a 90 wt% nanothermite using a simple direct-writing approach. The key additive in the ink is a hybrid polymer of poly(vinylidene fluoride) (PVDF) and hydroxy propyl methyl cellulose (HPMC) in which the former serves as an energetic initiator and a binder, and the latter is a thickening agent and the other binder, which can form a gel. The rheological shear-thinning properties of the ink are critical to making the formulation at such high loadings printable. The Young's modulus of the printed stick is found to compare favorably with that of poly(tetrafluoroethylene) (PTFE), with a particle packing density at the theoretical maximum. The linear burn rate, mass burn rate, flame temperature, and heat flux are found to be easily adjusted by varying the fuel/oxidizer ratio. The average flame temperatures are as high as ≈ 2800 K with near-complete combustion being evident upon examination of the postcombustion products.

Unlike CHNO energetic materials (in which the fuel and oxidizer are mixed at the molecular length scale), nanothermites, or "metastable intermixed composites," are heterogeneous pyrotechnics using nanometer-sized fuel (aluminum) and oxidizer (CuO, Fe₂O₃, Bi₂O₃, etc.) particles.^[1,2] They have found applications as soldering materials,^[3] igniters,^[4] propellants,^[5] as well as energetic additives in explosives due to their higher energy density in comparison to CHNO energetics.^[6–11] While high particulate loading can be found in polymer composites these systems involve relatively large super-micron particles.^[12] Nanometallic fuels in contrast have been limited by significant processing challenges because integration of nanoparticles into polymers significantly increases viscosity making traditional casting methods unfeasible as well as limiting additive manufacturing approaches. As such

Dr. H. Wang, Prof. M. R. Zachariah
Department of Chemical and Environmental Engineering
The University of California
Riverside, CA 92521, USA
E-mail: mrz@engr.ucr.edu

J. Shen, D. J. Kline, N. Eckman, N. R. Agrawal, T. Wu, P. Wang
Department of Chemical and Biomolecular Engineering and Department
of Chemistry and Biochemistry
The University of Maryland
College Park, MD 20742, USA

 The ORCID identification number(s) for the author(s) of this article can be found under <https://doi.org/10.1002/adma.201806575>.

DOI: 10.1002/adma.201806575

nanothermites have found limited implementation because particle loadings are not sufficient to obtain high energy densities.^[8,13–15]

One method by which to resolve the increased viscosity is to assemble these nanoparticles into microspheres while retaining their nanoscale features.^[7,13,14,16] Recently, there is an emerging interest in using additive manufacturing methods to prepare structural energetic materials via templating,^[17] melting-extruding,^[18] inkjet-printing,^[19] electrophoretic deposition,^[20] photopolymerization,^[12] foaming,^[21] and more. Among the many methods, direct-writing of solvent based inks is of particularly high interest due to its relative simplicity and convenience,^[22–25] moreover, the safety of the energetic materials can be dramatically enhanced upon addition of the solvent. In

a common ink, polymeric binders are used to provide structural integrity to the energetic formulations and afford mechanically stable, relatively insensitive, machinable and formable energetic architectures. Since binders are generally nonenergetic, it is preferred that the binder be added in the minimum quantity necessary as to maintain the desired mechanical properties. In the last few decades, hydroxyl-terminated polybutadiene (HTPB) has found common use as the binder in solid propellant, however, the curing time is too long (days) to be used for the direct-writing approach^[26–28] unless employing an external solidifying approach such as UV curing.^[12] New binders or binder hybrids are desired to achieve high particle loading and high energy density.

Here, we develop an ink formulation with only 10 wt% of polymers which can bind a 90 wt% nanothermite using a simple direct-writing approach. The ability to have such high particle loadings would significantly open up new avenues for practical application and implementation of nanothermites which have thus far been unavailable. Adjustment of fuel-oxidizer ratio, the reactivity, as measured by flame temperature, linear burn rate, and energy release rate, can be easily tuned.

An ideal formulated ink would enable high loadings of nanoparticulates in a reactive binder with a solvent that had reasonable vapor pressure, and such that the resulting structure has mechanical integrity suitable for the application of interest. Necessarily this implies that the ink should be shear thinning, but beyond this at such high loadings unless an extended network is generated the material will effectively print as a powder

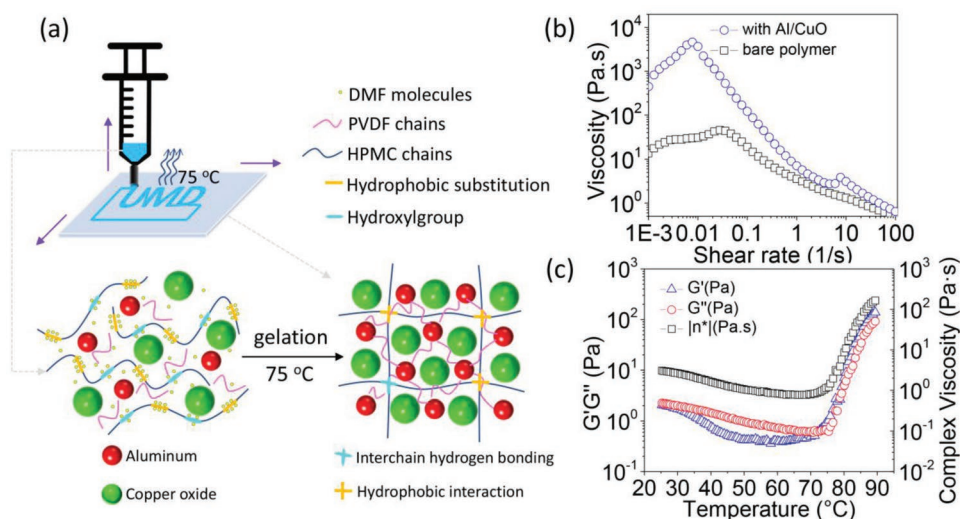


Figure 1. a) Gelation process in 3D-printing; b) rheology (apparent ink viscosity as a function of shear rate) of inks (bare PVDF/HPMC solution and with 90 wt% stoichiometric Al/CuO case); c) storage modulus (G'), loss modulus (G''), and complex viscosity (η^*) as a function of temperature (bare PVDF/HPMC solution); PVDF: HPMC mass ratio is 2:3.

with no cohesive strength. We found that to satisfy both the reactive and structural requirements required two binders; a polymer hybrid of hydroxy propyl methyl cellulose (HPMC, Methocel) and poly(vinylidene fluoride) (PVDF) with a mass ratio of 3:2. Both polymers are soluble in dimethyl formamide (DMF), and the hybrid mix was found to be very stable with no evidence of separation. PVDF was employed as a polymeric binder since it doubles as an oxidizer and improves the ignitability of the composite by promoting the preignition of Al relative to other soluble fluorine containing polymers such as Viton and THV.^[29] HPMC was chosen since it is known to gel via hydrophobic interactions occurring between hydrophobic segments of the polymer chains upon thermal treatment. The very low mass loading of HPMC employed mitigates the fact that it has minimal energy content. This effectively is increasing the degree of cross-linking between polymer chains, forming a continuous 3D network,^[30] as schematically shown in **Figure 1a**. For this demonstration we will fabricate an Al/CuO based thermite since this combination has been very commonly studied.^[1,5,7,8,13,16,17,20] CuO NPs (≈ 40 nm) and Al NPs (≈ 80 nm, ≈ 81 wt% active) were separately dispersed into the solution by ultrasonication and stirring for 24 and 1.5 h, respectively, resulting in the 90 wt% nanothermite ink. **Figure 1b** shows the ink viscosity versus shear rate of three inks with and without nanothermite. The apparent viscosity of pure polymer solution is in the scale of 10 Pa s, and dramatically increases by two to three orders of magnitude upon addition of solids. However, and most important for this application, the ink viscosity is highly dependent on shear rate. These inks show shear-thickening and -thinning behavior at low (<0.01 1 s^{-1}) and high shear rate (>0.05 1 s^{-1}), respectively. With the increase of shear rate, the viscosity of all the inks initially increases, but then demonstrates a sharp decline over several orders of magnitude. The PVDF in DMF solution was found to behave like a Newtonian fluid in low shear rate (constant viscosity with the increase of shear rate when <1 1 s^{-1}) while the HPMC in DMF solution shows a shear-thinning effect.^[31,32] The interactions between

PVDF and HPMC chains might contribute to the increase at low shear rate, however, the interactions could be easily destroyed due to interfacial slip between PVDF and HPMC at higher shear rates. The ink was extruded through an 18 Gauge needle (inner diameter is ≈ 1 mm) at a shear rate of rate $\approx 15\text{ s}^{-1}$ ($\approx 5.3\text{ mL h}^{-1}$) which corresponds to a dynamic viscosity of $\approx 1\text{--}2$ Pa s (**Figure 1b**).^[33,34] The ink was directly written in pre-designed patterns (programmed by G-code) on a preheated (≈ 75 °C) glass plate. This thermal treatment is implemented to induce the gelation of HPMC, and evaporation of the solvent (DMF) to form a complete dry layer before a second layer is written. In a typical sol-gel process, gelation refers to the critical point where viscosity dramatically increases.^[30] The storage (G') and loss (G'') modulus represent the elastic and viscous contributions, respectively. A higher storage modulus (G') relative to the loss modulus (G'') denotes a more solid-like property, where the critical point is observed at ≈ 75 °C in **Figure 1c**. The complex viscosity (considering both storage and loss modulus) reduced slightly from room temperature to 70 °C, and then has a very sharp increase > 2 orders of magnitudes for temperatures ≥ 75 °C, and can be defined as the gelation point. The rheological results of neat HPMC solution show the similar gelation temperature (≈ 75 °C) while the viscosity of PVDF solution remains roughly constant with temperature (before 85 °C), revealing that HPMC plays the key role in the gelation in this study (**Figure S1**, Supporting Information). This is further confirmed by the rheological result for ink with 90 wt% Al/CuO (**Figure S1**, Supporting Information).

Two primary patterns were employed to evaluate the print, one is a square (**Figure 2a**, top) of 8 cm \times 8 cm, and the other is a “UMD” pattern (**Figure 2b**, top) with a length of ≈ 5 cm and a width of ≈ 2 cm. The printed square was sufficiently mechanically sound as to enable it to be peeled off from the substrate and cut into ≈ 3 cm long sticks for burn rate measurement (**Figure 2a**, bottom). For each experiment, the sticks were weighed, and the accurate length was recorded. The width of the stick is largely dependent to the diameter of the needle

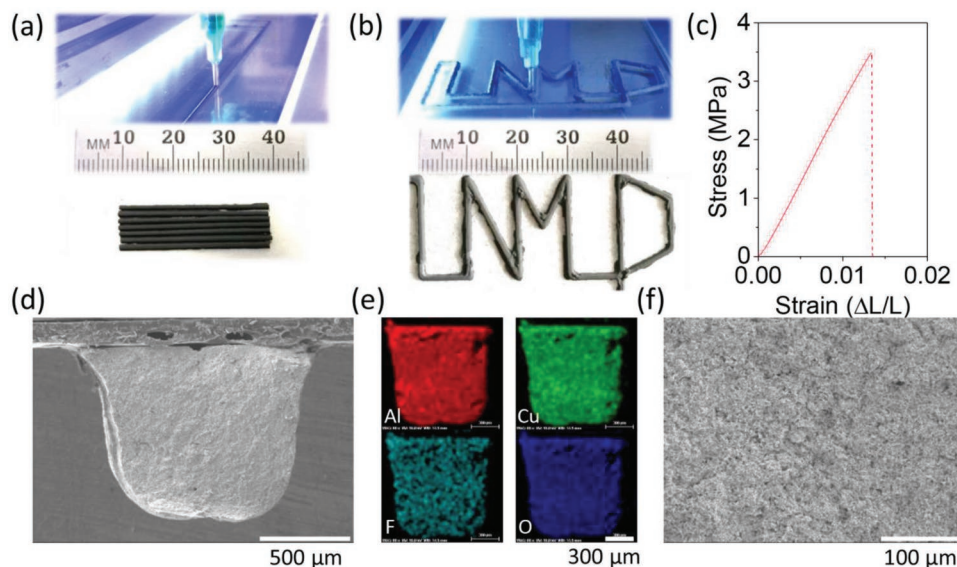


Figure 2. a,b) Photos of printed burn sticks (a) and UMD pattern (b) with stoichiometric Al/CuO. c) Stress–strain curves of printed burn sticks (with stoichiometric Al/CuO). d,f) Typical SEM images with low (d) and higher magnification (f). e) EDS results of the cross-sectional sticks (15 layers) (with 60 wt% Al in Al/CuO). All the samples contain 90 wt% of Al/CuO nanothermites, 4 wt% of PVDF and 6 wt% of HPMC.

(≈ 1 mm in diameter). The mechanical properties of the sticks with stoichiometric Al/CuO are shown in Figure 2c (90 wt% nanothermite loading). The peak yield stress is ≈ 3.5 MPa with a maximum strain ($\Delta L/L$) of 0.013, resulting in Young's modulus of ≈ 0.3 GPa, which is close to that of pure poly(tetrafluoroethylene) (PTFE).^[35] Importantly, this implies that the 90% loading nanothermite composite is mechanically sound.

To evaluate the density and to observe microstructure of the printed burn sticks, cross-section measurements using scanning electron microscopy (SEM) was employed. Combining the data of area, length and mass, the density and porosity of the burn sticks can be estimated.^[36,37] For the fuel lean and stoichiometric Al/CuO case, the densities were found to be ≈ 2.1 and ≈ 1.8 g cm⁻³, respectively, which is $\approx 1/3$ of the theoretical density. With the increase of Al content, the theoretical and actual density declined gradually owing to the lower density of Al compared to CuO, however, the porosity remains constant at $\approx 66\%$. While this may seem low, in fact the theoretical maximum packing density of nanoparticle aggregates is effectively this number, implying that the composite cannot be made denser. (Table 1).^[38,39] A higher packing density could be achieved if the nanoparticles are preprocessed to break the aggregates. The low (Figure 2d,f) and high (see the Supporting Information) magnification SEM images of the cross-sectional sticks also confirm the close packing of these nanoparticles in the printed burn sticks. The Al (≈ 80 nm) and CuO (≈ 40 nm) NPs were also confirmed to be intimately mixed (Figure 2e and the Supporting Information).

As previously mentioned, two polymeric binders (PVDF, HPMC) were investigated for incorporation into the high-loading Al/CuO ink. If the total polymer content and particles loading was fixed, replacing part of HPMC with PVDF would not only improve the ignitability but also reduce the viscosity of the ink. Considering the ratio between PVDF and HPMC might also play a significant role in both printing quality and

combustion performance, different inks (Table S1, Supporting Information) with five different PVDF/HPMC ratios (10:0 to 0:10; total polymer is fixed as 10 wt%) were prepared, and the corresponding “UMD” and sticks (15 layers) were printed (Figures S2 and S3, Supporting Information). The samples prepared with on PVDF based inks (10 wt%) were found to be very brittle and were difficult to remove from the substrate. On the other hand, samples without PVDF and only 10 wt% HPMC could not propagate in an Ar environment because HPMC alone is not energetic and presumably passivates the particles from reacting with each other. We found the best compromise to be a 4% PVDF and 6 wt% HPMC mix, which also had the best printing resolution and fewest defects. For subsequent results the formulation was fixed to 4 wt% PVDF and 6 wt% HPMC.

As a nanothermite ignites, the large heat release provides heat feedback to support flame propagation. The measured ignition temperature of the printed burn sticks measured by a fast-heating wire is as low as ≈ 550 °C (Figure S5, Supporting Information),^[13,14,29] which is close to that of Al/PVDF, further

Table 1. Measured density, theoretical density and porosity of the burn sticks with 90 wt% nanothermite loading (with different Al content from 10 to 90 wt%).

Al% in Al/CuO	Density [g cm ⁻³]	Bulk Density [g cm ⁻³]	Porosity [%]
10 ($\Phi = 0.3$)	2.1	5.50	63
22 ($\Phi = 1$)	1.8	5.12	65
30 ($\Phi = 1.5$)	1.7	4.85	65
40 ($\Phi = 2.3$)	1.4	4.53	70
50 ($\Phi = 3.5$)	1.4	4.20	67
60 ($\Phi = 5.3$)	1.3	3.88	67
70 ($\Phi = 8.2$)	1.0	3.55	72
80 ($\Phi = 14.1$)	1.1	3.22	66

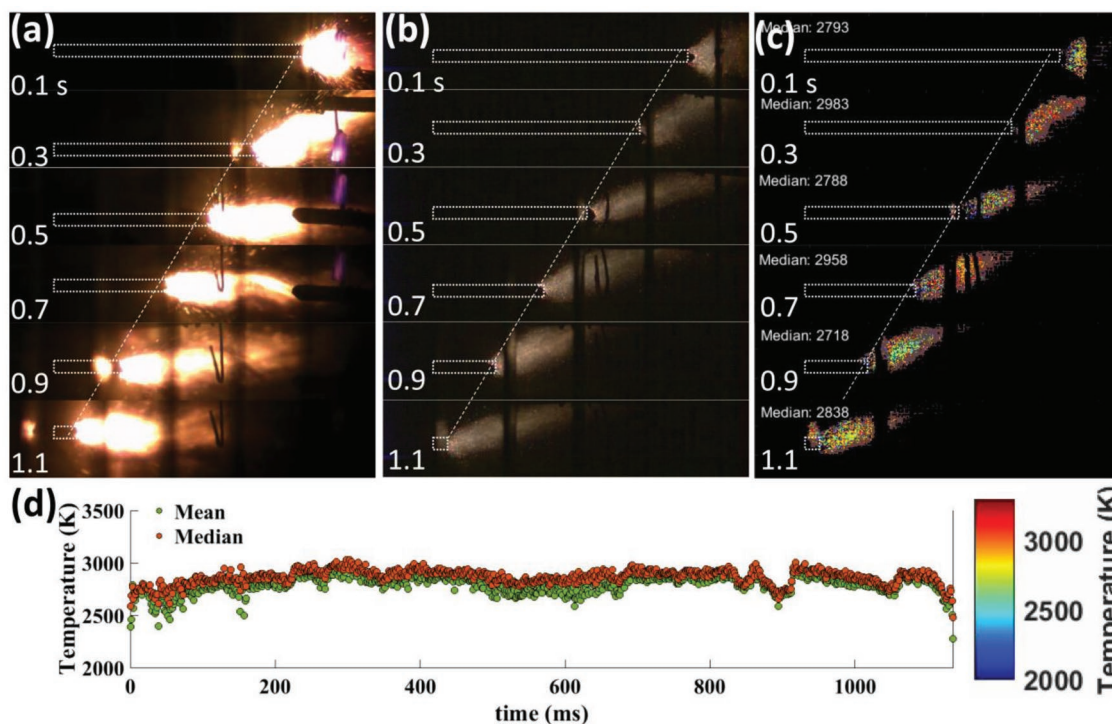


Figure 3. a,b) Burning snapshots with normal exposure (a) and low exposure (b). c,d) The measured temperature map (c) and curve (d) with time for 15-layered stick with 90 wt% Al/CuO nanothermite loading (6 wt% Methocel, 4 wt% PVDF, Al in Al/CuO is 22 wt%). The white dotted rectangles represent the burn stick.

confirming the advantage of PVDF. For the pure thermite Al/CuO, the adiabatic flame temperature is estimated as ≈ 2840 K and is limited by the boiling point of Cu (≈ 2835 K), one of the major reaction products.^[40] The flame propagation of the printed burn sticks (≈ 3 cm) with normal and low exposure along with the flame temperature maps, are shown in **Figure 3a–c**, and the detailed time-resolved mean/median flame temperature seen in **Figure 3b,d**. The latter was obtained using a high-speed color camera pyrometry technique detailed in our previous study.^[41] All combustion tests were conducted in 1 atm Ar to exclude the effect of additional oxygen.^[42] The horizontally propagating flame (**Figure 3a**) indicates very vigorous combustion, generating a large amount of hot gas/particles and a bright flame. The flame fronts proceed steadily (**Figure 3a–c**) with time and demonstrate a stable linear burn rate of ≈ 3 cm s^{-1} . Flame temperature remains steady over the length of the burn at 2500–3000 K, and most points located at ≈ 2800 K. This result is interesting in that it implies we can print a thermite-based material that has a measured flame temperature close to that theoretically expected (≈ 2843 K) and implying the polymer is not impeding the combustion process.^[40] The printed “UMD” was also ignited and the propagation on the glass slides was captured by high-speed imaging (see Videos S1–S3 and **Figure S6**, Supporting Information). Due to the heat convection and advection from fast moving hot gas/particles released in the combustion,^[20,40] when the flame approaches corners (such as the top of “M”), it jumps to the nearby unburnt part (when distance is < 0.5 cm).

Uniform burning of energetic materials is very important metric, as any abnormality in a solid propellant may lead to catastrophic failure.^[43] To evaluate the impact of thickness on

physical properties (morphology and density) and reactivity, Al/CuO/PVDF/HPMC ($\Phi = 1$) burn sticks with 5, 10, and 15 layers were prepared (see **Figure S7** in the Supporting Information for SEM images) and characterized. We find that morphology (see the Supporting Information) and density (≈ 1.8 g cm^{-3}) as shown in **Figure 4a** are effectively constant as are the burning properties (**Figure 4b**).

Generally, for nanothermites peak reactivity is achieved at or near stoichiometric.^[44] As shown in **Table 1** a range of equivalence ratios for Al/CuO were fabricated to investigate the impact of stoichiometry on reactivity. Cross-section SEM images (see **Figure S8**, Supporting Information) of different Al content from 10–80 wt% show similar morphology with a close packing of nanoparticles. **Figure 5** presents burn rate and temperature measurements as a function of Al/CuO ratio at 90% loading. The flame temperature peaks at ≈ 22 wt% of Al corresponding to the stoichiometric case ($\Phi = 1$), while the linear burn rate peaks at fuel rich (**Figure 5**, **Figures S9** and **S10**, Supporting Information), which is probably due to the enhanced gas production and heat convection with more reactive fuel.^[20,40] The energy release rate (normalized heat flux, estimated as the product of flame temperature and mass burn rate) in **Figure 5** peaks between the maximum flame temperature and burn rate implying that if optimization of energy release is desired, a fuel rich formulation ($\Phi = 1.5$ – 3.5) is necessary, despite its lower burn rate. Combustion product examined by XRD (**Table 2**, see **Figure S11** (Supporting Information) for detailed XRD patterns), find that the major products for stoichiometric Al/CuO are Cu and Al_2O_3 , indicating complete combustion. Under lean conditions there is an appreciable quantity of Cu_2O observed,

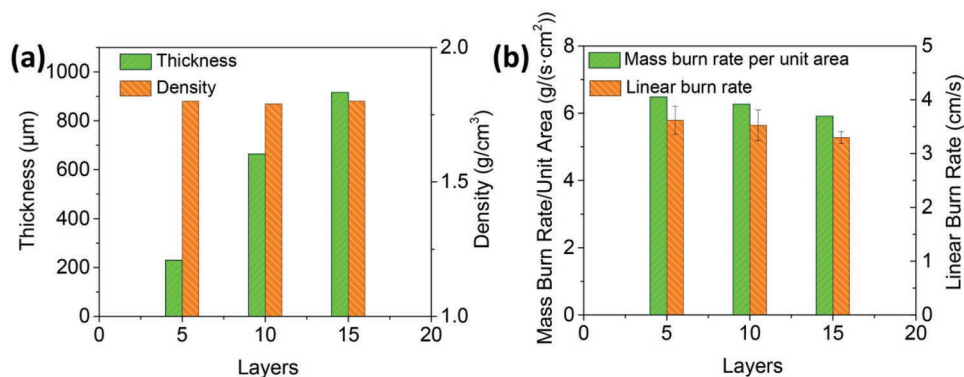


Figure 4. a) Measured thickness and density of 3D-printed burn sticks with 5, 10, and 15 layers. b) The mass burn rate per unit area and linear burn rate of 3D-printed sticks with 5, 10, and 15 layers. 90 wt% Al/CuO nanothermite loading (6 wt% Methocel, 4 wt% PVDF, Al in Al/CuO is 22 wt%, equivalence ratio of 1). One layer means one print path.

while under slightly rich conditions the presence of Cu_9Al_4 is present in the XRD pattern implying that the excess aluminum had sufficient time to alloy with copper. When the equivalence ratio is further increased to 5.3, we also see the alloy CuAl_2 .

In summary, we developed an energetic ink formulation with a particle loading of 90 wt% which can be used for direct writing of 3D structures. The key additive in the ink is a hybrid polymer of PVDF and HPMC, in which the former serves as an energetic initiator and a binder, and the latter is a thickening agent and the other binder which can adhere particles with a small percentage of polymer by forming a gel upon heating. The best polymer ratio (best printing resolution) was found to be 4 wt% PVDF and 6 wt% HPMC enabled particle loadings as high as 90 wt%. The rheology shear thinning properties of the ink was critical to make the formulation at such high loadings printable. The Young's modulus of printed stick is found to compare favorably with PTFE, with a particle packing density at the theoretical maximum. The linear burn rate, mass burn rate, flame temperature and heat flux were found to be easily adjusted by varying the fuel/oxidizer ratio. The average flame temperatures are as high as ≈ 2800 K with near-complete combustion being evident upon examination of the postcombustion products.

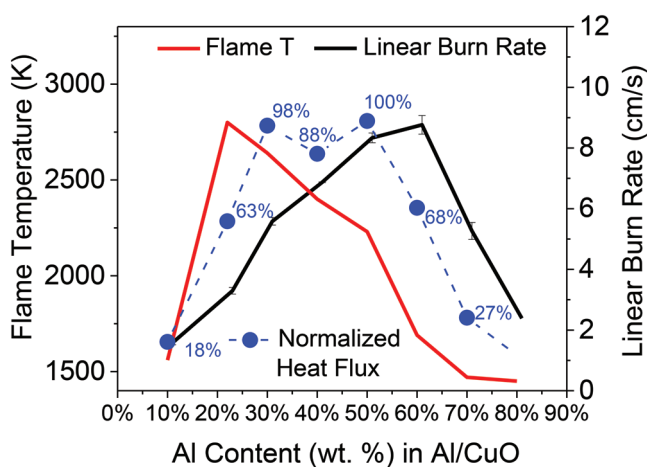


Figure 5. Linear burn rate, flame temperature, and normalized heat flux of the burn sticks with 90 wt% nanothermite loading (with different Al content in Al/CuO from 10 to 90 wt%).

Experimental Section

Chemicals: METHOCEL F4M hydroxypropyl methylcellulose (HPMC) was ordered from Dow Chemical Company. Poly(vinylidene fluoride) (PVDF, average molecular weight: $\approx 534\ 000$) and *N,N*-dimethylformamide (DMF, 99.8%) were purchased from Sigma-Aldrich. CuO nanoparticles (≈ 40 nm) were purchased from US Research Nanomaterials. Aluminum nanoparticles (Al NPs, ≈ 85 nm) were purchased from Novacentrix. The active aluminum content is ≈ 81 wt% according to thermogravimetry/differential scanning calorimetry (TG/DSC) results.

Ink Preparation and Rheological Tests: Different inks were prepared according to the following formations listed in Tables S1 and S2 (Supporting Information). When preparing the ink, certain amounts of HPMC and PVDF were first dissolved in DMF and magnetically stirred for ≈ 2 h to get a clear solution. Then the CuO and Al NPs were dispersed into the above polymer solution by ultrasonication for ≈ 1 h. The prepared slurry was then magnetically and mechanically stirred for 24 and 1.5 h, respectively, and the ink was ready to print. The rheological properties of the inks were characterized by an AR2000 rheometer mounted with a 40 mm 2" steel cone. A temperature ramp test was also performed with a $2\ ^\circ\text{C}\ \text{min}^{-1}$ rate of increase in temperature at $1\ \text{rad}\ \text{s}^{-1}$ angular frequency. The stress-strain was decided from the strain sweep test according to the linear viscoelastic (LVE) region at $25\ ^\circ\text{C}$.

T-Jump Ignition: Typically, a ≈ 10 mm long platinum filament ($\approx 76\ \mu\text{m}$ in diameter) was coated with the sample ($\approx 2\ \mu\text{m}$ thickness). The filament was resistively heated to ≈ 1400 K (heating rate of $\approx 4 \times 10^5\ \text{K}\ \text{s}^{-1}$, in 1 atm of Argon). The ignition and subsequent combustion of the composite was monitored using a high-speed camera ($14.9\ \mu\text{s}$ exposure with 256×256 pixels, Phantom V12.1, 76 000 pps). The temporal wire resistance (correlated via the Callendar-Van Dusen Equation) during the heating process was recorded and the ignition temperature was calculated by coupling the observed ignition timestamp from the high-speed video with the wire temperature.^[27]

Morphology Characterizations and Mechanical Tests: The microstructure of the printed samples was investigated by using a Hitachi SU-70 scanning electron microscope coupled to an energy-dispersive

Table 2. Species analysis of the combustion residues with different Al content from 10 to 60 wt%.

Al% in Al/CuO	Solid species by XRD
10 ($\Phi = 0.3$)	Cu, Cu_2O and Al_2O_3
22 ($\Phi = 1$)	Cu, $(\text{Al}_2\text{O}_3)_{5,3}$ and Al_2O_3
30 ($\Phi = 1.5$)	Cu, Cu_9Al_4 , $\text{AlAl}_{1.67}\text{O}_4$ ($\approx \text{Al}_2\text{O}_3$)
60 ($\Phi = 5.3$)	CuAl_2 , Cu_9Al_4 , Al_2O_3

spectrometer (EDS). The sticks were sectioned in liquid nitrogen and attached to a carbon film on a scanning electron microscope stage. The combustion products were also characterized by powder X-ray diffraction (XRD, Bruker D8 with Cu K radiation). Tensile strength of single layer films was measured using a Shimadzu Autograph AGS-X tensile tester.

Burning Rate and Flame Temperature Measurements: The sticks were cut into 3 cm sections for burning rate tests. They were ignited with a Joule-heated nichrome wire (spirally curved, 0.010 inches in diameter) in a quartz tube filled with argon in advance (10 L min⁻¹ argon flow for 5 min). The burning event was recorded using a high-speed camera at a rate of 7000 pps (Vision Research Phantom Miro M110 high-speed camera). The tests for each sample were conducted in triplicate and the average burning rate with standard error was reported.^[39]

To estimate temperature of the burning films, color ratio pyrometry was performed using the same high-speed color camera. By taking ratios of raw channel intensities, dependency on most variables associated with intensity is eliminated except for those regarding the channel gain, emissivity, and spectral response of the camera at individual wavelengths and channels. The camera was calibrated for temperatures ranging from 773–4773K with a Newport Oriol 67000 Series Blackbody Infrared Light Source using Planck's Law and the associated graybody assumption. MATLAB was used to extract raw pixel values and calculate temperatures. Three color ratios (green/red, blue/green, and blue/red) were simultaneously used to estimate temperature by minimizing their summed error from theoretical ratios with a nominal error less than ≈110K. For the figures that show temperature of a single level and within the error threshold are used to report mean/median temperature of the frame for a contiguous area of at least 10 acceptable pixels.^[40]

Supporting Information

Supporting Information is available from the Wiley Online Library or from the author.

Acknowledgements

This work was supported by the AFOSR. The authors acknowledge the support of the Maryland Nanocenter and its NispLab. The NispLab is supported in part by the NSF as an MRSEC Shared Experimental Facility.

Conflict of Interest

The authors declare no conflict of interest.

Keywords

3D printing, direct writing, energetic materials, high loading, nanothermites

Received: October 10, 2018

Revised: February 12, 2019

Published online: April 16, 2019

[1] E. Lafontaine, M. Comet, *Nanothermites*, ISTE Editions Ltd, London, UK **2016**.

[2] W. He, P. Liu, G. He, M. Gozin, Q. Yan, *Adv. Mater.* **2018**, *30*, 1706293.

[3] J. Yu, Y. Wang, W. Wen, D. Yang, B. Huang, J. Li, K. Wu, *Adv. Mater.* **2010**, *22*, 1479.

- [4] J. I. Gransden, M. J. Taylor, *Propellants, Explos., Pyrotech.* **2007**, *32*, 435.
- [5] S. Iyer, N. Slagg, *Adv. Mater.* **1990**, *2*, 174.
- [6] A. Prakash, A. V. McCormick, M. R. Zachariah, *Adv. Mater.* **2005**, *17*, 900.
- [7] S. H. Kim, M. R. Zachariah, *Adv. Mater.* **2004**, *16*, 1821.
- [8] E. L. Dreizin, *Prog. Energy Combust. Sci.* **2009**, *35*, 141.
- [9] M. Comet, C. Martin, M. Klaumünzer, F. Schnell, D. Spitzer, *Appl. Phys. Lett.* **2015**, *107*, 243108.
- [10] N. H. Yen, L. Y. Wang, *Propellants, Explos., Pyrotech.* **2012**, *37*, 143.
- [11] Y. Zhu, X. Zhou, J. Xu, X. Ma, Y. Ye, G. Yang, K. Zhang, *Chem. Eng. J.* **2018**, *354*, 885.
- [12] M. S. McClain, I. E. Gunduz, S. F. Son, *Proc. Combust. Inst.* **2019**, *37*, 3135.
- [13] H. Wang, G. Jian, G. C. Egan, M. R. Zachariah, *Combust. Flame* **2014**, *161*, 2203.
- [14] H. Wang, R. J. Jacob, J. B. DeLisio, M. R. Zachariah, *Combust. Flame* **2017**, *180*, 175.
- [15] U. Teipel, U. Förter-Barth, *Propellants, Explos., Pyrotech.* **2001**, *26*, 268.
- [16] F. Séverac, P. Alphonse, A. Estève, A. Bancaud, C. Rossi, *Adv. Funct. Mater.* **2012**, *22*, 323.
- [17] J. M. Slocik, R. McKenzie, P. B. Dennis, R. R. Naik, *Nat. Commun.* **2017**, *8*, 15156.
- [18] J. A. Bencomo, S. T. Iacono, J. McCollum, *J. Mater. Chem. A* **2018**, *6*, 12308.
- [19] A. K. Murray, W. A. Novotny, T. J. Fleck, I. E. Gunduz, S. F. Son, G. T. C. Chiu, J. F. Rhoads, *Addit. Manuf.* **2018**, *22*, 69.
- [20] K. T. Sullivan, C. Zhu, E. B. Duoss, A. E. Gash, D. B. Kolesky, J. D. Kuntz, J. A. Lewis, C. M. Spadaccini, *Adv. Mater.* **2016**, *28*, 1934.
- [21] M. Comet, C. Martin, F. Schnell, D. Spitzer, *Chem. Eng. J.* **2017**, *316*, 807.
- [22] S. Ghosh, S. T. Parker, X. Wang, D. L. Kaplan, J. A. Lewis, *Adv. Funct. Mater.* **2008**, *18*, 1883.
- [23] C. Chang, V. H. Tran, J. Wang, Y. Fuh, L. Lin, *Nano Lett.* **2010**, *10*, 726.
- [24] C. Xu, C. An, Y. He, Y. Zhang, Q. Li, J. Wang, *Propellants, Explos., Pyrotech.* **2018**, *43*, 754.
- [25] F. D. Ruz-Nuglo, L. J. Groven, *Adv. Eng. Mater.* **2018**, *20*, 1700390.
- [26] B. A. McDonald, J. R. Rice, M. W. Kirkham, *Combust. Flame* **2014**, *161*, 363.
- [27] R. Kurva, G. Gupta, K. I. Dhabbe, L. S. Jawale, P. S. Kulkarni, M. Maurya, *Propellants, Explos., Pyrotech.* **2017**, *42*, 401.
- [28] R. A. Chandru, N. Balasubramanian, C. Oommen, B. N. Raghunandan, *J. Propul. Power* **2018**, *34*, 1090.
- [29] H. Wang, M. Rehwoldt, D. J. Kline, T. Wu, P. Wang, M. R. Zachariah, *Combust. Flame* **2019**, *201*, 181.
- [30] K. K. Sadasivuni, J. J. Cabibihan, D. Ponnamma, M. A. Al-Maadeed, J. Kim, in *Biopolymer Composites in Electronics* (Eds: K. K. Sadasivuni, J. J. Cabibihan, D. Ponnamma, M. A. Al-Maadeed), Elsevier, New York, USA, **2017**, pp. 43–44.
- [31] X. Zhang, W. Lang, H. Xu, X. Yan, Y. Guo, *RSC Adv.* **2015**, *5*, 21532.
- [32] A. I. Barzic, R. M. Albu, L. M. Gradinaru, L. I. Buruiana, *e-Polymers* **2018**, *18*, 135.
- [33] K. A. Meeks, B. R. Clark, J. E. Cano, C. A. Apblett, M. L. Pantoya, *Combust. Flame* **2015**, *162*, 3288.
- [34] A. Allmendinger, S. Fischer, J. Huwyler, H. Mahler, E. Schwarb, I. E. Zarraga, R. Mueller, *Eur. J. Pharm. Biopharm.* **2014**, *87*, 318.
- [35] P. J. Rae, D. M. Dattelbaum, *Polymer* **2004**, *45*, 7615.
- [36] C. A. Schneider, W. S. Rasband, K. W. Eliceiri, *Nat. Methods* **2012**, *9*, 671.

- [37] C. Huang, G. Jian, J. B. DeLisio, H. Wang, M. R. Zachariah, *Adv. Eng. Mater.* **2015**, *17*, 95.
- [38] G. D. Scott, D. M. Kilgour, *J. Phys. D: Appl. Phys.* **1969**, *2*, 863.
- [39] C. Zangmeister, J. Radney, L.T. Dockery, J.T. Young, X. Ma, R. You, M.R. Zachariah, *Proc. Natl. Acad. Sci. USA* **2014**, *111*, 9037.
- [40] G. C. Egan, M. R. Zachariah, *Combust. Flame* **2015**, *162*, 2959.
- [41] H. Wang, J. B. DeLisio, S. Holdren, T. Wu, Y. Yang, J. Hu, M. R. Zachariah, *Adv. Eng. Mater.* **2018**, *20*, 1700547.
- [42] R. J. Jacob, D. J. Kline, M. R. Zachariah, *J. Appl. Phys.* **2018**, *123*, 115902.
- [43] M. Kumar, S. M. Kovacic, K. K. Kuo, *AIAA J.* **1981**, *19*, 610.
- [44] G. M. Dutro, R. A. Yetter, G. A. Risha, S. F. Son, *Proc. Combust. Inst.* **2009**, *32*, 1921.